Transition of the Radial Electric Field by Electron Cyclotron Heating in the CHS Heliotron/Torsatron

H. Idei,* K. Ida, H. Sanuki, H. Yamada, H. Iguchi, S. Kubo, R. Akiyama, H. Arimoto,† M. Fujiwara, M. Hosokawa, K. Matsuoka, S. Morita, K. Nishimura, K. Ohkubo, S. Okamura, S. Sakakibara, C. Takahashi, Y. Takita, K. Tsumori, and I. Yamada

National Institute for Fusion Science, Nagoya 464-01, Japan

(Received 16 February 1993)

The transition of a radial electric field from a negative to a positive value is observed in the compact helical system when the electron loss is sufficiently enhanced by the superposition of the off-axis second harmonic electron cyclotron heating on the neutral beam heated plasmas. Existence of the threshold for the enhanced particle flux required to cause the transition is experimentally certified. The observed threshold is compared with a theoretical prediction.

PACS numbers: 52.55.Hc, 52.50.Gj

A radial electric field near the plasma periphery has been found to play an important role in the improved confinement such as in the H-mode plasmas [1–3]. Theoretical models of the L/H transition in tokamaks have been proposed. It is predicted that the change in the radial electric field or in the plasma rotation has a strong influence on the transition [4–8]. In stellarator devices, the neoclassical theory suggests that the electric field reduces the helical ripple loss, and consequently improves the plasma confinement [9–11]. Multiple solutions of the electric field that satisfy the ambipolar constraint often arise when particle fluxes have a nonlinear dependence on the electric field. There are generally two stable states in the stellarator plasmas which are called the ion and the electron roots [11]. In a stellarator reactor, it is an important scenario to attain the electron root with higher energy confinement time through heating electrons in the start-up phase [9]. In a Heliotron-E device, the radial electric field at $r \simeq 0.7$–$0.9a$ is found to be positive (the electron root) for the low density plasma ($n_e < 1\times10^{13}$ cm^{-3}) and negative (the ion root) for the high density plasma ($n_e > 2\times10^{13}$ cm^{-3}) [12]. In the Wendelstein VII-A stellarator, the observed electric field in the plasma with electron cyclotron heating (ECH) ($n_e \sim 5\times10^{13}$ cm^{-3}) is consistent with a theoretical prediction [13]. In the advanced toroidal facility, the positive electric field is observed for the low density plasma with ECH ($n_e \sim 5\times10^{12}$ cm^{-3}) [14]. In the compact helical system (CHS) [15], the observed radial electric field is negative in the typical neutral beam (NB) heated plasmas [16]. The electric field becomes more negative near the plasma edge for the higher electron density.

It is generally observed that ECH has an effect of density pump-out both in tokamaks [17] and in stellarators [18,19]. In CHS, it is observed that the particle confinement becomes worse in the plasma with second harmonic ECH at low field side resonance than at high field side resonance [20]. One of the candidates to explain the mechanism of the density pump-out is the outward flux due to the poor confinement of perpendicularly accelerated electrons by ECH [21]. In this Letter, we present the transition of the radial electric field from the ion root to the electron root triggered by enhancing the electron particle flux with ECH.

CHS is a heliotron/torsatron device with a pole number of $l=2$, a toroidal period number $m=8$, and an aspect ratio of 5. The major radius R is 92 cm and the averaged minor radius a is 19 cm. The second harmonic ECH is carried out with the 53.2 GHz gyrotron of the maximum pulse width of 100 ms. Here, more than 60% of the injection power is focused into a beam with a 2.5 cm $1/e$ spot size on the midplane of a CHS vacuum vessel with a desired extraordinary mode. The focusing system is composed of a stair cut Vlasov antenna, an improved reflecting mirror, a reflecting corrugated polarizer, and a steerable focusing mirror [20]. The 7.5 MHz ion cyclotron range of frequency is used for the preionization of plasmas in this study [22]. The neutral beam is tangentially injected to sustain the plasmas and to utilize a charge exchange spectroscopy (CXS). Poloidal rotation and ion temperature are measured with CXS with a time resolution $\Delta t_{\mathrm{CXS}}=16.7$ ms [23]. The radial electric field is evaluated from the observed poloidal rotation and the ion pressure gradient using a radial momentum balance equation for a fully ionized carbon. In the momentum balance equation, a toroidal rotation has little contribution to the radial electric field, because the toroidal rotation damps due to a viscous damping force caused by the helical ripple [24].

The second harmonic ECH is superposed to an NB heated target plasma in order to enhance the electron particle flux. The density in the NB heated target plasma is controlled to stay below the cutoff density. The focus point of ECH is located at $r=0.5a$ in the low field side region, since the enhanced electron flux at the low field side resonance heating is expected to be larger than at the high field side resonance heating. A line-averaged electron density decreases with the superposition of ECH. The enhanced electron flux is controlled by changing the ECH injection power ($P_{\mathrm{ECH}}=85$, 105, and 140 kW). Figure 1 shows radial profiles of electron density $n_e(\rho)$ and temperature $T_e(\rho)$, measured with Thomson scatter-

0031-9007/93/71(14)/2220(4)$06.00

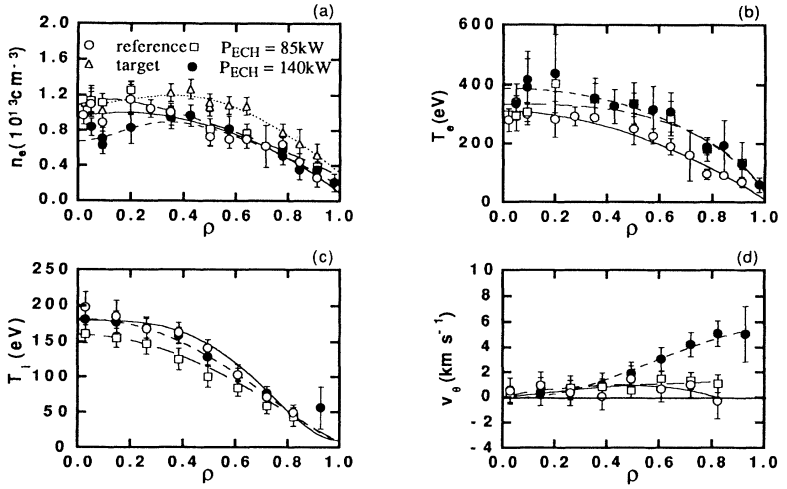

FIG. 1. Radial profiles of (a) electron density, (b) electron temperature, (c) ion temperature, and (d) poloidal rotation velocity for the reference plasma and those with the injection power $P_{ECH}=85$ and 140 kW. The electron density profile for the target plasma is also shown in (a).

ing (TS), ion temperature $T_i(\rho)$, and poloidal rotation velocity $v_\theta(\rho)$, measured with CXS at 15 ms after the ECH is turned on for the plasmas with $P_{ECH}=85$ and 140 kW, where ρ is a normalized radius calculated with finite β equilibrium code, VMEC [25]. The experiments for the plasmas with $P_{ECH}=85$, 105, and 140 kW are carried out for the target plasma with a fixed density ($\sim 9.5\times 10^{12}$ cm^{-3}). As a reference plasma, we choose the plasma such that the line-averaged density is adjusted to be as low as that for the plasma with $P_{ECH}=140$ kW to eliminate the density dependence of the radial electric field. Radial profiles $n_e(\rho)$, $T_e(\rho)$, $T_i(\rho)$, and $v_\theta(\rho)$ for the reference plasma and $n_e(\rho)$ for the target plasma are also shown in Fig. 1. The plasmas with $P_{ECH}=105$ and 140 kW rotate in the ion-diamagnetic direction which means the positive electric field, while the small rotation velocity is observed for the target plasma, the reference plasma, and that with $P_{ECH}=85$ kW.

Figure 2(a) shows time evolutions of the line-averaged densities for the target plasma $\bar{n}_e^{tar}(t)$, the reference plasma $\bar{n}_e^{ref}(t)$, and the plasma superposed by ECH, $\bar{n}_e(t)$. The profile of the enhanced particle flux $\Gamma_{ECH}(\rho)$ is deduced from the continuous equation using the density decay $\partial n_e(\rho,t_0)/\partial t$ after the ECH is turned on ($t=t_0$),

$$\Gamma_{ECH}(\rho)=\frac{a}{\rho}\int_0^\rho \rho'\frac{\partial n_e(\rho',t_0)}{\partial t}d\rho', \tag{1}$$

$$\frac{\partial n_e(\rho,t_0)}{\partial t}=\frac{\Delta\bar{n}_e(\infty)}{\tau_{nl}}\frac{n_e(\rho,t_1)-n_e^{tar}(\rho,t_1)}{\bar{n}_e(t_1)-\bar{n}_e^{tar}(t_1)}. \tag{2}$$

Here, $n_e^{tar}(\rho,t_1)$ and $n_e(\rho,t_1)$ are the electron density profiles measured with TS ($t=t_1$) for the target plasma and that superposed by ECH, respectively. $\Delta\bar{n}_e(\infty)/\tau_{nl}$ is given by the fitting of $\Delta\bar{n}_e(t)$ [defined as $\bar{n}_e(t)-\bar{n}_e^{tar}(t)$] as $\Delta\bar{n}_e(\infty)(1-\exp[-(t-t_0)/\tau_{nl}])$. Since the gas puffing rates are adjusted to be the same for both the target plasma and that superposed by ECH, the difference of the source term $\Delta S(\rho,t)$ [defined as $S(\rho,t)-S^{tar}(\rho,t)$] is neglected. At $t=t_1$, H_α intensity for the plasma superposed by ECH increases by about 20% of that for the target plasma due to the degradation of the particle confinement by ECH. The evaluated profiles $\Gamma_{ECH}(\rho)$

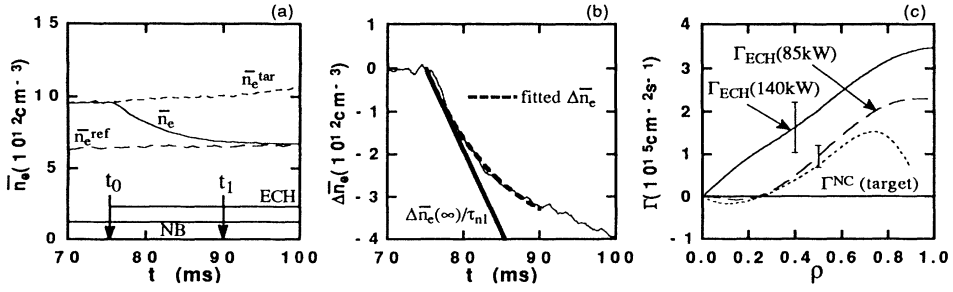

FIG. 2. Time evolutions of (a) line-averaged electron densities of the target plasma, the reference plasma, and that superposed by ECH, $\bar{n}_e^{tar}(t)$, $\bar{n}_e^{ref}(t)$, and $\bar{n}_e(t)$, and (b) the difference, $\Delta\bar{n}_e(t)\equiv\bar{n}_e(t)-\bar{n}_e^{tar}(t)$. (c) Radial profiles of enhanced fluxes Γ_{ECH} for the plasmas with the injection power $P_{ECH}=85$ and 140 kW, and a neoclassical flux Γ^{NC} for the target plasma.

are shown in Fig. 2(c) for the plasmas with $P_{ECH}=85$ and 140 kW. The error bars in Fig. 2(c) come from the fitted $\Delta\bar{n}_e(\infty)$ and τ_{nl}. Figure 2(c) shows also the profile of the neoclassical flux $\Gamma^{NC}(\rho)$ for the target plasma, which is estimated from the connection formula of neoclassical transport that covers the whole collisionality regime [Eqs. (6)-(11) in Ref. [10]] by using the fitting curves for $n_e(\rho)$, $T_e(\rho)$, and $T_i(\rho)$. For simplicity, we assume a single helicity model in the theoretical calculations. Both ions and electrons for the reference and the target plasma are in the plateau regime in the whole plasma region. For the plasma superposed by ECH, although ions are in the plateau regime, electrons are in the $1/\nu$ regime (electron collisionality ν_{*e} [is equal to $(qR/\varepsilon_h^{1.5}\times v_{th})\nu$] >0.5) at $\rho\simeq 0.6$-0.9. Here, ν is the pitch angle scattering frequency by the collisions, q is a safety factor, ε_h is the helical ripple, and v_{th} is a thermal velocity.

Figure 3(a) shows the observed radial electric field profiles for the reference plasma and that with $P_{ECH}=140$ kW. The large positive electric field is observed near the plasma edge for the plasma with $P_{ECH}=140$ kW(~ 44 V cm^{-1} at $\rho=0.82$). Figure 3(a) also shows the radial electric field profiles evaluated theoretically from an ambipolarity equation [26], $\Gamma_e^{NC}+\Gamma_{ECH}=\Gamma_i^{NC}$. Here, we assume that ECH enhances only electron particle flux, not ion particle flux. It is noted that the ambipolarity equation gives the upper limit of the radial electric field on each magnetic surface. The profile of the calculated electric field is not in agreement with that of the observed electric field for the plasma with $P_{ECH}=140$ kW. The calculated electric field is more positive at the plasma edge ($\rho>0.8$), and is more negative at the core region than the observed electric field. The ambipolarity equation may contain multiple solutions and causes the discontinuities in the electric field profile, because it is given on each magnetic surface. If the transition of the radial electric field occurs in the outer region, the electric field diffuses into the inner region under the influence of the perpendicular viscosity. Therefore, the theoretically evaluated electric field should become a more smooth radial profile such as that of the observed electric field by taking the diffusion process of the electric field into consideration. To explain the transition phenomena qualitatively, we restrict our results to the electric field at $\rho=0.82$. Figure 3(b) shows a dependence of the radial electric field on the enhanced flux Γ_{ECH} for various P_{ECH} at $\rho=0.82$. The transition of the radial electric field from a negative (the ion root) to a positive value (the electron root) is observed at the larger enhanced flux ($\sim 4\times 10^{15}$ cm^{-2}s^{-1}). Although the enhanced flux becomes large when the plasma is heated with the higher P_{ECH}, it does not change much even though the higher P_{ECH} is injected after the transition occurs. Since the obtained density and temperature profiles are different in this power scan experiment, the neoclassical fluxes estimated from the profiles change a little. The scattering of the theoretical predictions in Fig. 3(b) is caused by the change of the neoclassical fluxes.

Figure 3(c) shows the dependences of the ion and electron neoclassical fluxes on the radial electric field for the plasma with $P_{ECH}=140$ kW at $\rho=0.82$. The ion neoclassical flux strongly depends on the radial electric field E_r and has a peak at $E_r\simeq 0$ while the electron neoclassical flux has a weak dependence on the radial electric field. If the additional electron loss flux Γ_{ECH} is small, the ambipolarity constraint does not much affect the radial electric field. However, if Γ_{ECH} is increased and becomes large enough to have multiple solutions, the transition occurs.

Further technical improvement is required to show experimentally clear transition phenomena such that the electric field changes dramatically at a critical P_{ECH} during ramping up P_{ECH}. As for the theoretical model, we do not discuss the dependence of the enhanced flux Γ_{ECH} on the radial electric field. To understand the mechanism causing the enhanced flux is extremely important but is left to a future work.

In conclusion, the transition of the radial electric field is observed by sufficiently enhancing the electron flux with the second harmonic ECH in CHS. The observed

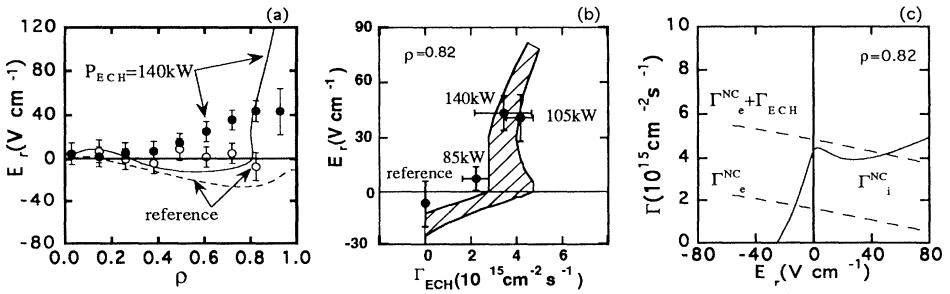

FIG. 3. (a) Radial electric field profiles for the reference plasma and that with the injection power $P_{ECH}=140$ kW. Open and closed circles show observed radial electric fields. Broken and solid curves show calculated ones. (b) Radial electric fields E_r versus enhanced fluxes Γ_{ECH} at $\rho=0.82$ for the plasmas with various P_{ECH}. Closed circles show the observed E_r and the hatched area represents the theoretical prediction. (c) Dependences of ion and electron neoclassical fluxes, Γ_i^{NC} and Γ_e^{NC}, on E_r for the plasma with $P_{ECH}=140$ kW at $\rho=0.82$.

transition is qualitatively explained by the theoretical model based on the ambipolarity equation.

One of the authors (H.I.) wishes to express his thanks to Dr. T. Watari for his encouragement and discussion. The authors would like to thank members of the torus experimental group for fruitful discussions and also to the technical staffs for the operation of ECH and NB systems. This work is partially supported by the Grant-in-Aid from the Ministry of Education.

---

*Present address: Department of Physics, Faculty of Science, Nagoya University, Nagoya 464-01, Japan.

†Present address: Plasma Science Center, Nagoya University, Nagoya 464-01, Japan.

[1] F. Wagner *et al.*, Phys. Rev. Lett. **49**, 1408 (1982).

[2] R. J. Groebner, K. H. Burrel, and R. P. Seraydarian, Phys. Rev. Lett. **64**, 3015 (1990).

[3] K. Ida *et al.*, Phys. Rev. Lett. **65**, 1364 (1990).

[4] S.-I. Itoh and K. Itoh, Phys. Rev. Lett. **60**, 2276 (1988).

[5] K. C. Shaing and E. C. Crume, Jr., Phys. Rev. Lett. **63**, 2369 (1989).

[6] H. Biglari, P. H. Diamond, and P. W. Terry, Phys. Fluids B **2**, 1 (1990).

[7] A. B. Hassam, T. M. Antonsen, Jr., J. F. Drake, and C. S. Liu, Phys. Rev. Lett. **66**, 309 (1991).

[8] F. L. Hinton, Phys. Fluids B **3**, 696 (1991).

[9] H. E. Mynick and W. N. G. Hitchon, Nucl. Fusion **23**, 1053 (1983).

[10] L. M. Kovrizhnykh, Nucl. Fusion **24**, 435 (1984).

[11] D. E. Hastings, W. A. Houlberg, and K. C. Shaing, Nucl. Fusion **25**, 445 (1985).

[12] K. Kondo *et al.*, Rev. Sci. Instrum. **59**, 1533 (1988).

[13] H. Wobig, H. Massberg, H. Renner, The WVII-A Team, the ECRH Group, and the NI Group, in *Plasma Physics and Controlled Nuclear Fusion Research, 1986, Kyoto* (IAEA, Vienna, 1987), Vol. II, p. 369.

[14] S. C. Aceto *et al.*, in *Proceedings of International Conference on Plasma Physics, Innsbruck, 1992,* Vol. 16C, Pt. I, p. 529.

[15] K. Matsuoka *et al.*, in *Plasma Physics and Controlled Nuclear Fusion Research, 1988, Nice* (IAEA, Vienna, 1989), Vol. II, p. 411.

[16] K. Ida, H. Yamada, H. Iguchi, S. Hidekuma, H. Sanuki, K. Yamazaki, and the CHS Group, Phys. Fluids B **3**, 515 (1991); **4**, 1360 (1992).

[17] H. Hsuan *et al.*, in *Heating in Toroidal Plasmas,* Proceedings of the Fourth International Symposium (International School of Plasma Physics, Varenna, 1984), Vol. 2, p. 809.

[18] F. Sardei, H. Ringler, A. Dodhy, G. Kühner, WVII-AS Group, and ECRH Group, in *Proceedings of 17th European Physical Society Conference on Controlled Fusion and Plasma Heating, Amsterdam, 1990* (European Physical Society, Petit-Lancy, 1990), Vol. 14B, Pt. II, p. 471.

[19] H. Zushi *et al.*, Nucl. Fusion **28**, 1801 (1988).

[20] S. Kubo *et al.*, in *Proceedings of International Conference on Plasma Physics* (Ref. [14]), p. 513.

[21] K. Itoh, S.-I. Itoh, and A. Fukuyama, J. Phys. Soc. Jpn. **58**, 482 (1989).

[22] O. Kaneko *et al.*, in *Plasma Physics and Controlled Nuclear Fusion Research, 1990, Washington* (IAEA, Vienna, 1991), Vol. II, p. 473.

[23] K. Ida and S. Hidekuma, Rev. Sci. Instrum. **60**, 876 (1989).

[24] K. Ida, H. Yamada, H. Iguchi, K. Itoh, and CHS Group, Phys. Rev. Lett. **67**, 58 (1991).

[25] H. Yamada *et al.*, Nucl. Fusion **32**, 25 (1992).

[26] H. Sanuki, K. Itoh, K. Ida, and S.-I. Itoh, J. Phys. Soc. Jpn. **60**, 3698 (1991).